Cross sections for the anisotropic interaction of NNO with various molecules

Cynthia J. Jameson
Department of Chemistry, University of Illinois at Chicago, Chicago, Illinois 60680

A. Keith Jameson and Joseph K. Hwang
Department of Chemistry, Loyola University, Chicago, Illinois 60626

Nancy C. Smith
Dexter Corporation, Midland Division, Waukegan, Illinois 60685

(Received 22 June 1988; accepted 28 July 1988)

Cross sections for the relaxation of the rotational angular momentum vector of the NNO molecule on collision with CO, Ar, CO_2, NNO, Kr, CF_4, and Xe, have been measured by ^{15}N spin relaxation in $^{15}N^{15}NO$ molecules. The relaxation times of the two nuclei are in a ratio 1.86, independent of density, collision partner, or temperature. Except for Ar and CO, the cross sections are larger than the hard sphere cross sections and their temperature dependences range from $T^{-0.8}$ to $T^{-1.0}$.

INTRODUCTION

In dilute gases of polyatomic molecules the phenomena which are directly related to the anisotropy of the intermolecular potential include angular momentum alignment phenomena and effects of collision on radiation absorption or scattering. Condensed phase experiments can also yield information about the intermolecular potential, but these are not nearly so explicitly described by theory. In the dilute gas, kinetic theory allows each of these properties to be described in terms of an effective cross section which can be calculated in terms of collision integrals or matrix elements of the scattering or transition operator for a given intermolecular potential. For most molecules the rotational levels are sufficiently closely spaced for a classical or semiclassical calculation at temperatures near room temperature or higher.

Of the angular momentum alignment phenomena, nuclear spin relaxation offers the possibility of exploring the same potential surface with more than one probe nucleus effectively providing redundant information or additional information, e.g., $^{15}N^{15}NO$ with $^{13}CO_2$. Furthermore, relaxation due to unlike pair collisions can be characterized nearly as precisely as that due to like pairs, in contrast with viscosity, effects of fields on transport properties, or flow birefringence. The cross sections obtained in NMR relaxation, as in these other properties, are averaged over the J and M_J quantum numbers, unlike the pressure broadening of pure rotational absorption or rotational Raman lines, which are J-state labeled. Unlike the field effects on transport properties, the factors which relate the effective cross section to the observed NMR relaxation times are completely defined and well known from Gordon's theory,[1,2] and the molecular constants involved are independently directly measureable.

The NNO molecule was chosen for spin relaxation studies for several reasons. NNO is isoelectronic with CO_2 and its electric quadrupole moment is only slightly smaller than that of CO_2,[3] and it has a small dipole moment, so that comparisions of cross sections obtained from ^{15}N and ^{13}C spin relaxation studies should provide insight into the types of information the cross sections provide. Secondly, for the central nitrogen in NNO there is a discrepancy in the values of the spin–rotation constant which are obtained from chemical shifts and from molecular beam electric resonance spectroscopy.[4] The ratio of the spin relaxation rates of the two ^{15}N nuclei gives the ratio of the squares of their spin–rotation constants, which allows us to resolve this discrepancy. Finally there are several other observables which can be used together with our T_1 data for a determination of a potential surface by a multiproperty fit. Several cross sections for NNO–NNO are available from other properties and a selected few for NNO–Ar, NNO–N_2, and NNO–CO_2. The structures of NNO–HF and NNO–Ar van der Waals complexes have been elucidated spectroscopically.[5,6] Infrared and Raman band shapes of NNO mixed with rare gases have been measured in dense gas phase[7–10] and the rotational time-correlation functions for these systems have been characterized in terms of the empirical mean square torque.[8,11] The latter is theoretically explicitly known if the anisotropic intermolecular potential is known. An intermolecular potential function for NNO–Ar based on the Gordon–Kim electron gas model gives good agreement with the mean square torque measurements at high temperature and with the geometry of the van der Waals complex.[11] The scaling factors which relate the spherical average potential of NNO–NNO, NNO–Ar, NNO–N_2, and NNO–CO_2 to that of Ar–Ar have been determined from binary viscosity and diffusion coefficients in these gas mixtures.[12]

EXPERIMENTAL

Experimental details have been previously described[13,14] except for the following. Isotopically enriched $^{15}N^{15}NO$ gas (95 at. % ^{15}N) was obtained from MSD isotopes. The measurements reported here were made in an IBM WP-200SY and a Bruker AM400 NMR spectrometer using broadband probes tuned to ^{15}N at 20.3 and 40.5 MHz, respectively. An example of an inversion recovery experiment on a pure NNO sample is shown in Fig. 1. The pulse sequence $(\pi$–delay time–$\pi/2$–wait $5T_1)_n$ was used; each spectrum is labeled with the variable delay time. 0.3 μs is effectively a delay time of zero, and 18 s in this case is effectively infinitely long for complete recovery of the magnetization of both ^{15}N nuclei in the molecule. Typically, however, a

 0021-9606/88/215642-08$02.10

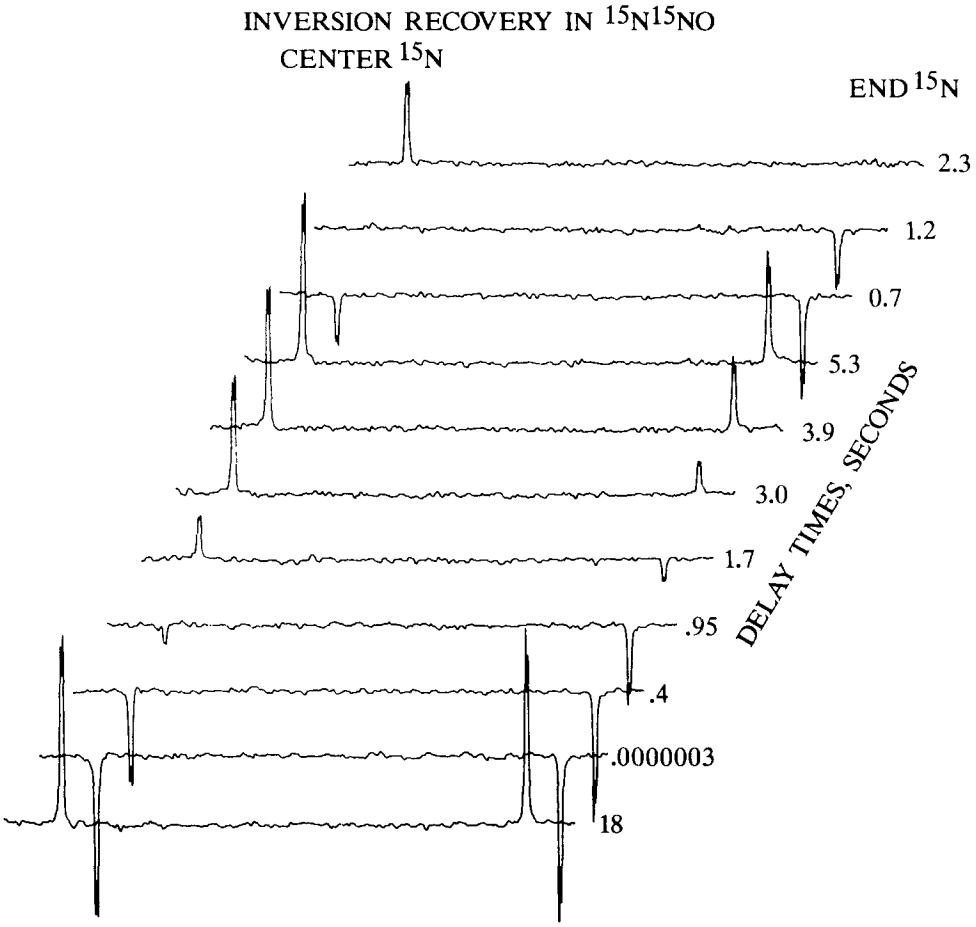

FIG. 1. ^{15}N spectra in NNO gas; the numbers are delay times τ in the inversion recovery pulse sequence (π–τ–$\pi/2$).

line broadening parameter is chosen large enough so as to obliterate the fine splitting due to spin–spin coupling observed in Fig. 1. The irradiation frequency (central frequency) lies exactly between the two chemically shifted ^{15}N nuclei, approximately 1800 Hz from each. There is a very small transmitter attenuation at this offset from each peak. This routinely leads to a required 2% increase in pulse width to obtain π and $\pi/2$ pulses at this 1800 Hz offset. This was accounted for. Since the center nucleus relaxes almost twice as fast as the end one, a composite list of delay times was used, using the shortest delays necessary for the central ^{15}N, the longest delays needed for the end ^{15}N, and compromise intermediate delay times. Each T_1 measurement takes many hours since T_1 is long (seconds). Systematic changes which may arise from variation in spectrometer conditions over this period of time are converted into data scatter by using a list of delay times which are not in ascending order and by cycling. That is, an intermediate number of transients is taken, e.g., 32, for a chosen delay list and stored. The same number of transients is taken again and added to those previously stored until the desired total number of transients is reached (e.g., 256 transients are taken in 8 loops of 32). In processing the data, all FIDs are weighted with the same exponential function, and the absolute intensity is used so that all spectra are scaled in intensity to A_∞. Typical data are shown in Fig. 2. The relaxation time increases with decreas-

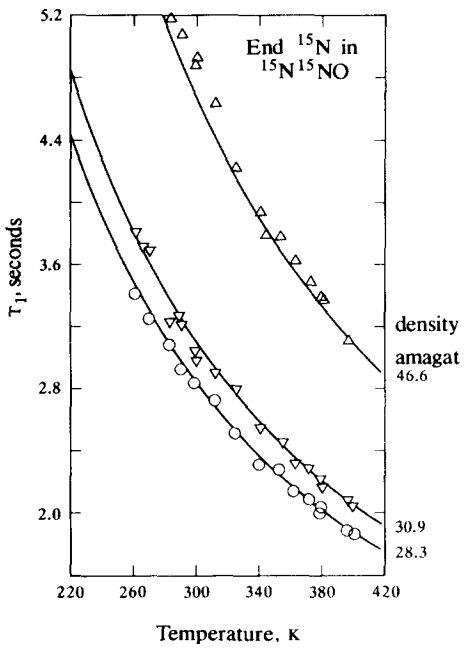

FIG. 2. Typical results of inversion recovery experiments for ^{15}N in $^{15}N^{15}NO$ gas. These data are for the end ^{15}N in three samples of pure NNO, taken at 40.5 MHz. The curves are given by a function resulting from a two-parameter fit to all points for all samples of pure NNO, assuming a power law, $T_1 = (T_1/\rho)_{300\,K}\,(T/300)^n\rho$, where $n = -1.417$.

ing temperature as expected. The relative standard deviation in T_1 is typically less than 1% at 40.5 MHz and about 3% at 20.3 MHz. In using a composite delay list, all the delays are appropriate for the end nucleus, while the long delays used for the end nucleus are much too long for the central nucleus. A slight misestimation of the expected relaxation times can mean that very few of the delay times used in an experiment are useful in determining the relaxation time of the central nucleus. Thus, the relaxation times of the end nucleus are somewhat better defined than those of the central nucleus.

RESULTS

The results obtained here are for intermediate densities where the "extreme narrowing limit" is attained (collision frequency $\gg$ Larmor precession frequency) and the gas may still be considered dilute (binary collision regime). Nuclear spin relaxation times have been related by Gordon[1] to the explicit properties of binary collisions between molecules in gas densities low enough that the duration of a collision is short compared to the average time between collisions. Gordon has shown that[1]

$$\frac{1}{T_1^{\mathrm{SR}}} = \frac{2}{3}\omega_{\mathrm{SR}}^2 \langle \mathbf{J}^2 \rangle \tau_J , \tag{1}$$

where ω_{SR} is the spin–rotation constant (in radians per second) in the interaction Hamiltonian between the nuclear spin angular momentum $\mathbf{I}$ and the rotational angular momentum $\mathbf{J}$ of the molecule (both in units of $\hbar$):

$$H_{\mathrm{SR}} = \hbar\omega_{\mathrm{SR}} \mathbf{I}\cdot\mathbf{J} , \tag{2}$$

$$\omega_{\mathrm{SR}} = 2\pi C_\perp , \tag{3}$$

with $C_\perp$ in Hz. $\langle \mathbf{J}^2 \rangle$ is the average square rotational angular momentum which in NNO can be taken to be the classical limit,

$$\langle \mathbf{J}^2 \rangle = \frac{2I_0 kT}{\hbar^2} = \frac{kT}{B_0} . \tag{4}$$

The most important effect of the collisions is to cause transitions between the internal states J and M_J of the molecule. In the pure gas of density ρ, the correlation time τ_J is given by[1]

$$\tau_J = (\rho\bar{v}\sigma_J)^{-1} , \tag{5}$$

where $\bar{v}$ is the mean relative velocity and σ_J the cross section. $\rho\bar{v}\sigma_J$ is the rate of the collision-induced transitions ($\Delta J \neq 0$ and/or $\Delta M_J \neq 0$) in NNO. For a mixture of NNO with other gases, it is found that

$$T_1^{\mathrm{SR}} = (T_1/\rho)_{\mathrm{NNO\text{-}NNO}}\,\rho_{\mathrm{NNO}} + (T_1/\rho)_{\mathrm{NNO\text{-}X}}\,\rho_{\mathrm{X}} . \tag{6}$$

This observed additivity depends on the lack of correlation between the effects of successive collisions and also on the assumption of binary collisions.

The results are summarized in Table I. Note that the ratio of (T_1/ρ) values for the end and center nuclei is fairly constant for each NNO–buffer pair and is roughly 2. So long as the ^{15}N relaxation is completely dominated by the spin–rotation mechanism in $^{15}N^{15}NO$, the relaxation rates of the two ^{15}N nuclei are related to the ratio of the squares of their spin–rotation constants:

$$\frac{(T_1^{-1})_{\mathrm{cen}}}{(T_1^{-1})_{\mathrm{end}}} = \frac{(C_1^2)_{\mathrm{cen}}}{(C_1^2)_{\mathrm{end}}} .$$

A plot of the T_1 ratios is shown in Fig 3, showing the invariance of the ratio with temperature, density, or collision partner, verifying the dominance of the spin rotation mechanism and indicating that the effects of rovibrational averaging and intermolecular interactions on the spin–rotation constants of ^{15}N in NNO are relatively small. As discussed below, this is supported by the previous studies of ^{15}N chemical shifts in this molecule in mixtures of gases,[15] and in the zero-pressure limit,[16] which are consistent with the measured temperature dependence of the rovibrationally averaged structural parameters.[17] The average of the ratios of the relaxation times of the end to the center nuclei in NNO from Fig. 3 is 1.86. The spin–rotation constants $C_{\perp\mathrm{cen}} = 4.15$ kHz and $C_{\perp\mathrm{end}} = 2.48$ kHz from molecular beam electric resonance spectra[18] give a ratio of 2.80:1, which is not in agreement with the data in Fig. 3. The absolute shielding scale (based on the nitrogen spin rotation constants in NH_3), on the other hand, yields $\sigma = 11.3$ ppm (cen) and 99.5 ppm (end) which correspond to spin–rotation constants 3.35 kHz (cen) and 2.47 kHz (end).[4] The ratio of these is 1.84:1 (shown as the horizontal line in Fig. 3) which agrees with the spin relaxation data. Since the spin–rotation constants for the end nitrogen are in excellent agreement, the constant for the central nitrogen in NNO from molecular beam data is very likely in error. It has previously been pointed out that the molecular beam data are inconsistent with the observed internal chemical shift between the end and center nitrogen nuclei in this molecule.[4] For this work we will use the values $C_{\perp\mathrm{cen}} = 3.35$ kHz and $C_{\perp\mathrm{end}} = 2.48$ kHz.

We can estimate the magnitudes of the temperature and density dependence of $C_\perp$. From the relationship[19]

$$\frac{C_\perp}{B_0} = 3\frac{m_e}{m_p} g\sigma^{\mathrm{SR}}$$

TABLE I. ^{15}N spin relaxation times for NNO in various buffer gases. $T_1 = (T_1/\rho)_{300\,\mathrm{K}} \cdot (T/300)^{-n} \cdot \rho_{\mathrm{X}}$.

X	$(T_1/\rho)_{\mathrm{cen}}$ at 300 K (s amagat^{-1})	$(T_1/\rho)_{\mathrm{end}}$ at 300 K (s amagat^{-1})	n	T (K)
CO	0.0349 ± 0.0013	0.0644 ± 0.0025	− 1.315 ± 0.047	235–400
Ar	0.0363 ± 0.0021	0.0663 ± 0.0039	− 1.365 ± 0.063	235–400
CO_2	0.0538 ± 0.0033	0.1024 ± 0.0068	− 1.440 ± 0.108	255–400
NNO	0.0540 ± 0.0011	0.1005 ± 0.0019	− 1.417 ± 0.014	240–400
Kr	0.0447 ± 0.0045	0.0828 ± 0.0072	− 1.461 ± 0.111	230–400
CF_4	0.0579 ± 0.0015	0.1060 ± 0.0046	− 1.371 ± 0.069	255–400
Xe	0.0491 ± 0.0042	0.0899 ± 0.0064	− 1.417 ± 0.129	285–400

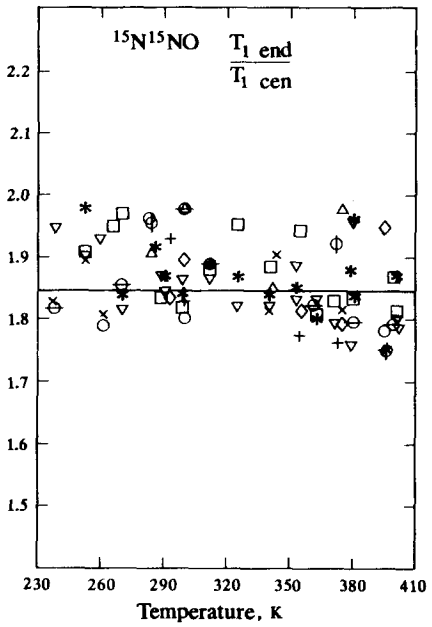

FIG. 3. The ratio of ^{15}N T_1 values in each experiment at 40.5 MHz in samples of pure NNO and of NNO in mixtures with the gases reported here. The horizontal line is the expected ratio if the ^{15}N spin–rotation constants derived from the nitrogen shielding scale are correct.

for a linear molecule, and the approximation $\sigma^{SR} \cong \sigma - \sigma(\text{free atom})$, the temperature and density dependence of nuclear shielding,

$$\sigma(T,\rho) = \sigma_0(T) + \sigma_1(T)\rho + \cdots$$

gives rise to

$$\frac{1}{C_\perp}\frac{dC_\perp}{dT} \cong \frac{1}{\sigma_0}\left(\frac{d\sigma_0}{dT} + \rho\frac{d\sigma_1}{dT}\right)$$

and

$$\frac{1}{C_\perp}\frac{dC_\perp}{d\rho} \cong \frac{\sigma_1}{\sigma_0}.$$

For the end ^{15}N nucleus in NNO,

$$\frac{d\sigma_0}{dT} = -8.5\times10^{-3} \text{ ppm deg}^{-1},^{15}$$

$$\sigma_0(300 \text{ K}) = 99.5 \text{ ppm},^{4}$$

and the largest measured value of σ_1 for NNO is that for end ^{15}N in NNO in xenon gas in which[15]

$$\sigma_1(300 \text{ K}) = -0.016 \text{ ppm amagat}^{-1}$$

and

$$\frac{d\sigma_1}{dT} = +6.3\times10^{-5} \text{ ppm amagat}^{-1} \text{ deg}^{-1}.$$

Thus, we expect $C_\perp$ for the end ^{15}N to change by 0.8% for a temperature change of 100 deg and by 0.5% for a density change of 30 amagat. These systematic changes in the spin–rotation constant are too small to be observed in Fig. 3. On the other hand, the introduction of oxygen provides a second relaxation mechanism and makes the ratio systematically smaller than 1.86. The ratio drops to 1.66 and 1.34 upon introduction of 3 and 26 amagats of O_2. (This is the subject of a separate study.)

We show the temperature dependence of T_1 for both the ^{15}N nuclei in one sample of pure NNO in Fig. 4. The ^{15}N(cen) data have been offset by an amount $\ln(C_\perp^2)_{cen}/(C_\perp^2)_{end}$ in this plot. The lines shown are the independent least-squares fits to the central and end N relaxation data separately. We see that both sets of data exhibit the same temperature dependence. All data for the three samples shown in Fig. 2 can reasonably be fitted by the same straight line of slope -1.42 ± 0.02. The slopes of these plots for the other NNO–buffer pairs and the values of (T_1/ρ) at 300 K are summarized in Table I.

CROSS SECTIONS FOR ANGULAR MOMENTUM TRANSFER σ_J

Cross sections for angular momentum transfer have been calculated from the spin relaxation data using Eqs. (1)–(5) and their values at 300 K are shown in Table II. On the basis of Fig. 3 and the above discussion, we use the spin–rotation constants $(C_\perp)$ 2.48 kHz (end) and 3.35 (center), and a classical average $\langle \mathbf{J}^2 \rangle = kT/B_0$ where the rotational constant is 0.4048 cm^{-1}.[20] The cross sections should be independent of which nucleus in the molecule is used as a probe; the same changes in the rotational angular momentum of the molecule are sensed by both end and central nucleus. Indeed we find in Fig. 5 that the cross sections obtained from the end and central nuclei agree within experimental error if these spin–rotational constants obtained from nuclear shielding are used. Figure 6 shows the temperature dependence of the cross sections for NNO with various collision partners.

For comparison between cross sections of different collision pairs the cross sections may be reduced by the size of the molecules. The definition of a reduced cross section is somewhat arbitrary. For internal consistency we have used the related scaling parameters from the extended law of corre-

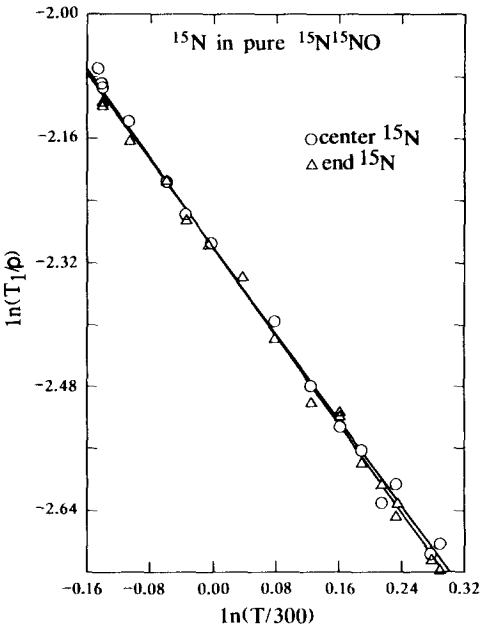

FIG. 4. The temperature dependence of T_1/ρ for the end ^{15}N and the central ^{15}N are the same, as they should be. A direct comparison is made possible by offset of the central ^{15}N data points by an amount $\ln(C_{end}^2/C_{cen}^2)$. Only the data points for the 28.3 amagat sample are shown in this plot.

TABLE II. Cross sections (σ_J) for changes in the rotational angular momentum vector at 300 K, obtained from relaxation times, this work.

Collision pair	Cross sections, Å^2		m[b]	Collision efficiency $= \sigma_J/\sigma_{geom}$	
NNO–X	σ_J(300 K)	σ_{geom}[a]		NNO–X	CO_2–X[c]
NNO–CO	33.1 ± 1.3	41.796	0.81 ± 0.05	0.72	···
NNO–Ar	37.7 ± 2.2	38.528	0.86 ± 0.06	0.98	0.83
NNO–CO_2	59.8 ± 3.9	43.685	0.94 ± 0.11	1.37	1.34
NNO–NNO	59.34 ± 1.1	43.078	0.91 ± 0.01	1.377	···
NNO–Kr	55.6 ± 4.8	41.671	0.96 ± 0.11	1.33	1.2
NNO–CF_4	71.7 ± 3.1	53.872	0.87 ± 0.07	1.33	···
NNO–Xe	64.6 ± 4.7	45.604	0.92 ± 0.13	1.4	1.4

[a] Calculated from πr_0^2 using r_0(NNO–X) from Kestin and Ro(Ref. 12) for NNO–N_2, NNO–Ar, NNO–CO_2, and NNO–NNO. All others are calculated using arithmetic mean of r_0 of like pairs, data from Table A3.2 of G. C. Maitland, M. Rigby, F. B. Smith, W. A. Wakeham, *Intermolecular Forces their Origin and Determination* (Clarendon, Oxford, 1981).

[b] The curves in Figs. 5 and 6 are the functions $\sigma_J(T) = \sigma_J(300\text{ K})(T/300)^{-m}$.

[c] Reference 13.

sponding states in this and in previous work.[13,14] These are at least uniformly derived from experiment by a well-defined relation and the values for like and unlike pairs are independently obtained. In Table II we present the cross sections for NNO–X pairs obtained in this work and the reduced cross sections which can be considered as collision efficiencies for changes in the rotational angular momentum vector of NNO molecules. These values are close to unity; almost every collision causes a change in the rotational angular momentum vector. The list of buffers is ordered in increasing polarizability. The collision efficiency increases with increasing polarizability (with a few exceptions), indicating these data are sensitive to the attractive part of the potential. NNO is an unusually effective collision partner among the buffer gases studied in this work. NNO has a small dipole moment so that electrostatic forces are longer range (falling off as R^{-3} with another $C_{\infty v}$ molecule or R^{-4} with a $D_{\infty h}$ molecule) and induction forces are no longer zero.[21] The relatively high efficiency of NNO–CO_2 and NNO–NNO collisions may

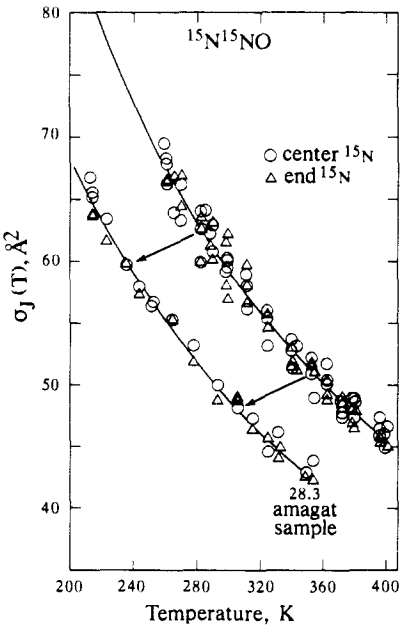

FIG. 5. The temperature dependence of the cross section $\sigma_J(T)$ for NNO. The curve is the function 59.34 $(T/300)^{-0.91}$ Å^2. Also shown are the data points for one sample only, to indicate (by difference) that part of the error in the cross sections reported in this work are due to errors in determination of sample density.

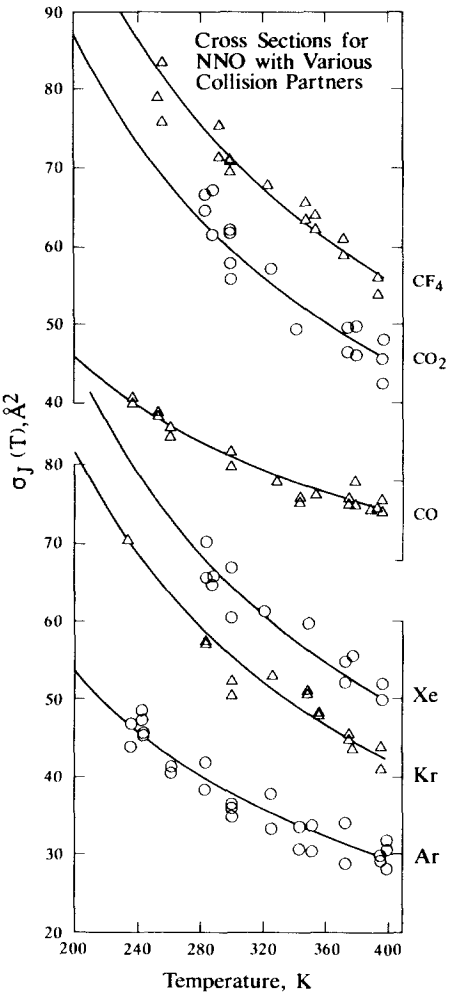

FIG. 6. The temperature dependence of the cross section $\sigma_J(T)$ for NNO with various collision partners. Data were obtained at 20.3 and 40.5 MHz. The curves are the functions given in Table II.

partly be attributed to the contribution of dipole–quadrupole electrostatic forces in these pairs. However, the anisotropy of the NNO–X intermolecular potential includes the short-range anisotropy which could be more important.

COMPARISON WITH OTHER CROSS SECTIONS

Our cross sections σ_J are compared with other cross sections for NNO in Table III. As defined by the Chen, Moraal, and Snider coupling scheme,[22] using modified notation,[23] in the classical limit σ_J is the same as $\sigma'(0\hat{1})$. A review of the experimental data and their relation to the cross sections shown in Table III is given by Ref. 24.

The other cross section which may be obtained from NMR relaxation times is σ_θ or $\sigma'(0\hat{2})$. This is obtained from the quadrupolar relaxation of ^{14}N nuclei in $^{14}N^{14}NO$ as opposed to the spin–rotation–relaxation of ^{15}N nuclei in $^{15}N^{15}NO$. For ^{14}N nuclei,

$$T_1 = \frac{160I^2(2I-1)}{3(2I+3)}\left(\frac{\hbar}{eqQ}\right)^2 \rho\bar{v}\sigma_\theta \,. \tag{7}$$

The nuclear quadrupole coupling constant $(eqQ/\hbar)$ has to be independently known. The same molecular beam experiment from which was obtained the spin–rotation contants of ^{14}N (converted to ^{15}N) yields $(eqQ/\hbar)$ for both ^{14}N nuclei.[18] Here again there appears to be a discrepancy. The ratio $(T_1^{-1})_{end}/(T_1^{-1})_{cen}$ for quadrupolar relaxation is found experimentally to be 6.1 in the gas phase and independent of density.[25] Theoretically, this ratio should be identical to the ratio $(eqQ)^2_{end}/(eqQ)^2_{cen}$. The latter is 8.36 from molecular beam spectroscopy;[18] it is apparent that one or both $(eqQ/\hbar)$ values are in error. Since the spin–rotation constant for the center nucleus is inconsistent with shielding and is probably in error, the same may hold for $(eqQ/\hbar)$. Thus, we assume that $(eqQ/\hbar) = 773.76$ kHz for ^{14}N (end) is correct (and the value for the other is too small). We use this value to calculate the cross section $\sigma_\theta = 53$ Å, shown in Table III.

The cross sections σ^{RA} from pressure broadening of pure rotational absorption in NNO[26] are found to be in reasonably good agreement with calculations[27] based on the Anderson–Tsao–Curnutte theory, including quadrupole–quadrupole and dipole–quadrupole interactions, using a molecular electric quadrupole moment equal to 6 Buckingham(b), $\mu = 0.166$ D, and $r_0 = 3.88$ Å. (One Buckingham is 10^{-26} esu cm^2 $= 10^{-40}$ C m^2/0.299 79 in SI units.) The linewidth data of Toth are somewhat different and the same theory leads to a quadrupole moment equal to 8.4 b.[28] However, independently measured values of the quadrupole moment are about half as large. The quadrupole moment of NNO derived from the dielectric second virial coefficient

TABLE III. Comparison of various cross sections for NNO–NNO collisions, at 293 except where noted.

Observable	Relaxation of[a]	Cross section	Å^2	Ref.	CO_2–CO_2(Å^2)	Ref.
Bulk viscosity	internal energy	$\sigma(0001)$	14.70(308 K)	34(a)	15.99(308 K)	34(a)
Sound absorption	rotational energy	$\sigma_{rot}(0001)$	27[b]	24	27[b]	24
					33.9(298 K)	34(b)
Thermal conductivity	relative velocity	$\sigma(10E)$	37.1(300 K)	24	38.8	24
Shear viscosity	relative velocity	$\sigma(20)$	52.4[c]	35	52.2	35
	alignment		52 ± 1[c]	36		
Spin–rotation relaxation time	angular momentum direction	$\sigma'(0\hat{1})$	59(^{15}N)(300 K)	this work	59.9	13
^{14}N quadrupolar spin–relaxation time	angular momentum alignment direction	$\sigma'(0\hat{2})$	53[d]	25		
Depolarization Rayleigh (DPR) line broadening	angular momentum alignment direction	$\sigma(0\hat{2})$	···		90.2	24
					88	39
Viscomagnetic effect	angular momentum alignment direction	$\sigma(02\pi)$	64	36	68,69	36,39
Magnetic field effect on thermal conductivity		$\sigma(12q)$	···		86	24
Pure rotational dipolar absorption		σ^{RA}	144[e,f]	37		
			190[e,f]	38		
			123–205[f]	28		

[a] In the classical limit.

[b] Calculated by Ref. 24 from a rotational collision number $Z_{rot} = 1.3$–2.0 (Ref. 40) using $\sigma_{rot}(0001) = (4/\pi)(kT/\bar{v})1/\eta(1/Z_{rot})$ (Ref. 41). On the other hand, Ref. 34(a) cites $Z_{rot} = 1.95$ at 300 K for CO_2.

[c] Calculated using $\sigma(20) = (kT/\bar{v})/\eta$.

[d] Calculated from ^{14}N NMR relaxation time measured in 15 atm gas (Ref. 25) using (Ref. 1) $T_1 = 160[I^2(2I-1)/3(2I+3)](\hbar/eqQ)^2\rho\bar{v}\sigma$, using the value of $(eqQ/\hbar)$ for the end ^{14}N in NNO from molecular beam results (Ref. 18).

[e] For $J = 5 \rightarrow 6$ line of NNO. Also NNO–Ar 88 Å^2, NNO–CO_2 134 Å^2, NNO–N_2 111 Å, (Ref. 3 and 27), and, for $J = 0 \rightarrow 1$ line of NNO, NNO–CO_2 150 Å^2, NNO–N_2 127 Å^2 (Ref. 38).

[f] Calculated from linewidths using $\sigma = (2\pi/\rho\bar{v})(\Delta\nu)_{1/2}$.

(3.4 b)[29] agrees well with that obtained by Buckingham *et al.* from induced birefringence in the gas (3.5 b).[3]

Other pressure-broadening results are available for NNO.[7,8,30,31] Unlike that of pure rotational spectra, the line shape analysis of a vibrational band does not allow a direct connection between peak width and cross section since the first and second moment of a parallel vibrational band depends entirely on the rotational constants of the vibrational levels.[32] From the density-dependent second and fourth moments may be obtained a mean square torque $\langle(\mathbf{O}V)^2\rangle$ which for NNO–Rg (Rg = rare gas) binary interactions can be related to the intermolecular potential $V(r,\theta)$, as in Ref. 7:

$$\langle(\mathbf{O}V)^2\rangle = \rho 2\pi \int_0^\infty \int_0^\pi \left(\frac{\partial V}{\partial \theta}\right)^2 \times \exp(-V/kT) r^2\, dr \sin\theta\, d\theta\,. \qquad (8)$$

O is an operator whose components along the inertial axes represent derivatives with respect to angles of rotation about the inertial axes. Like the cross sections obtained in this work, $\langle(\mathbf{O}V)^2\rangle/\rho$ arises entirely from the anisotropy of the intermolecular potential. Line shape analysis of the ν_3 band of NNO in Ar at total densities 50–250 amagat finds $\langle(\mathbf{O}V)^2\rangle$ is directly proportional to ρ at each temperature (which indicates binary NNO–Ar interactions are dominant even at these densities) and its *increase* with temperature shows that the anisotropy of the repulsive part of the intermolecular potential is largely responsible for the torque. The mean square torque on NNO by X is increasing in this order of X:[33] $He < H_2 < Ar < O_2 < N_2 < CH_4$.

COMPARISON OF NNO WITH CO_2

In Table II, comparison is made with the corresponding collision efficiencies of CO_2–X pairs. The cross sections in Tables II and III are essentially the same for NNO–NNO and CO_2–CO_2 for a wide variety of experiments, which is not surprising since the masses, moments of inertia, and even the electric quadrupole moments and polarizabilities of NNO and CO_2 are very similar. Millat *et al.* have derived a consistent set of effective cross sections for CO_2 and NNO from thermal conductivity and viscosity data in the range 308.15 to 426.15 K. These include $\sigma(0001)$, $\sigma(1001)$, $\sigma(1010)$, $\sigma(2000)$, and $\sigma(10E)$. These cross sections for NNO are very similar to and systematically below those for CO_2 (by no more than 5%). However, NNO does have a small electric dipole moment and a more anisotropic potential so that we might expect to find in some cases that $\sigma(\text{NNO–X}) > \sigma(\text{CO}_2\text{–X})$. Thus, we plotted σ_J for NNO–X and for the corresponding CO_2–X and found that while σ_J for the like pairs and with each other (that is, NNO–NNO, NNO–CO_2, CO_2–CO_2) are nearly identical, σ_J for NNO–Ar, Kr, Xe are greater than σ_J for CO_2–Ar, Kr, Xe, respectively. These are shown in Fig. 7. Since CO_2 and NNO are very similar in mass, moments of inertia, and size, these differences may be attributed largely to the greater anisotropy of the NNO–X potential compared to the CO_2–X potential.

Determination of a potential surface by multiproperty analysis generally means a fit to molecular beam scattering,

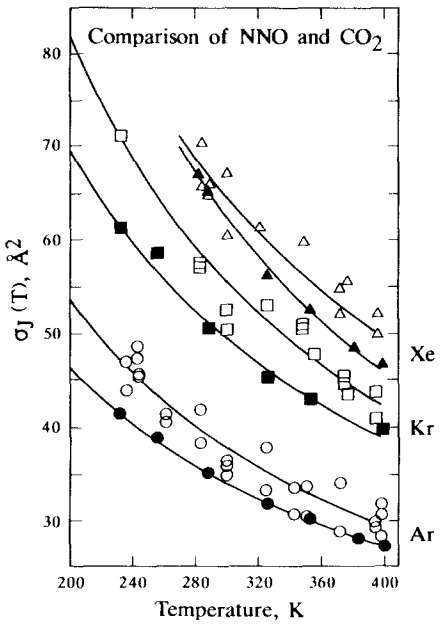

FIG. 7. Comparison of cross sections of NNO and CO_2 in collisions with rare gas atoms (filled symbols for CO_2, open symbols for NNO).

second virial coefficients, viscosity, and spectra of van der Waals molecules. For NNO and CO_2 there is considerably more information [as shown in Table III and given in Ref. 34(a)] which are directly related to the anisotropy of the potential. These relaxation data and other angular momentum alignment phenomena should be taken into account. Taken together with the mean square torque, these data can lead to a more precise determination of the anisotropy of the potential surfaces describing the interaction of NNO or CO_2 with another molecule.

ACKNOWLEDGMENT

This research has been supported in part by the National Science Foundation (Grant No. CHE85-05725).

[1] R. G. Gordon, J. Chem. Phys. **44**, 228 (1966).
[2] R. G. Gordon, J. Chem. Phys. **45**, 1635, 1649 (1966).
[3] A. D. Buckingham, R. L. Disch, and D. A. Disch, J. Am. Chem. Soc. **90**, 3104 (1968).
[4] C. J. Jameson, A. K. Jameson, D. Oppusunggu, S. Wille, P. M. Burrell, and J. Mason, J. Chem. Phys. **74**, 81 (1981).
[5] A. M. Sapse and J. M. Howell, J. Chem. Phys. **78**, 5738 (1983).
[6] C. H. Joyner, T. A. Dixon, F. A. Baiocchi, and W. Klemperer, J. Chem. Phys. **75**, 5285 (1981).
[7] C. Dreyfus and J. Cartigny, J. Chem. Phys. **80**, 5388 (1984).
[8] C. Dreyfus, R. Ouillon, and L. Berreby, J. Chem. Phys. **78**, 5379 (1983).
[9] N. Lacome and A. Levy, J. Mol. Struct. **80**, 257 (1982).
[10] L. Berreby and E. Dayan, Mol. Phys. **48**, 581 (1983).
[11] C. Dreyfus, D. Balou, and N. Brigot-Dutartre, J. Chem. Phys. **80**, 5393 (1984).
[12] J. Kestin and S. T. Ro, Ber. Bunsenges. Phys. Chem. **86**, 948 (1982).
[13] C. J. Jameson, A. K. Jameson, N. Smith, and K. Jackowski, J. Chem. Phys. **86**, 2717 (1987).
[14] C. J. Jameson, A. K. Jameson, and N. C. Smith, J. Chem. Phys. **86**, 6833 (1987).
[15] C. J. Jameson, A. K. Jameson, H. Parker, S. M. Cohen, and C. L. Lee, J. Chem. Phys. **68**, 2861 (1978).
[16] C. J. Jameson and H. J. Osten, J. Chem. Phys. **81**, 2556 (1984).
[17] B. R. Miller and M. Fink, J. Chem. Phys. **83**, 939 (1985).

[18]J. M. L. J. Reinartz, W. L. Meerts, and A. Dymanus, Chem. Phys. **31**, 19 (1978).
[19]W. H. Flygare, J. Chem. Phys. **41**, 793 (1964).
[20]C. Amiot, J. Mol. Spectrosc. **59**, 380 (1976).
[21]A. D. Buckingham, Adv. Chem. Phys. **12**, 107 (1967).
[22]F. M. Chen, H. Moraal, and R. F. Snider, J. Chem. Phys. **57**, 542 (1972).
[23]E. Mazur, J. J. M. Beenakker, and I. Kuscer, Physica A **121**, 430 (1983).
[24]H. Van Houten, L. J. F. Hermans, and J. J. M. Beenakker, Physica A **131**, 64 (1985).
[25]R. E. Wasylishen (private communications).
[26]R. M. Goody, J. Opt. Soc. Am. **58**, 904 (1968).
[27]G. D. T. Tejwani and P. Varanasi, J. Quant. Spectrosc. Radiat. Transfer **11**, 1659 (1971).
[28]R. A. Toth, J. Mol. Spectrosc. **40**, 588, 605 (1971).
[29]S. Kirouac and T. K. Bose, J. Chem. Phys. **59**, 3043 (1973).
[30]N. Van Thanh, J. P. Bouanich, and I. Rossi, Mol. Phys. **40**, 869 (1980).
[31]R. Ouillon, Chem. Phys. Lett. **35**, 63 (1975).
[32]R. G. Gordon, J. Chem. Phys. **39**, 2788 (1963); **41**, 1819 (1964); Adv. Magn. Reson. **3**, 1 (1968).
[33]M. Chalaye, E. Dayan, and G. Levi, Chem. Phys. Lett. **8**, 337 (1971).
[34](a) J. Millat, M. Mustafa, M. Ross, W. A. Wakeham, M. Zalaf, Physica A **145**, 461 (1987); (b) J. Millat, A. Plantikow, D. Mathes, and H. Nimz, Z. Phys. Chem. (Leipzig) (in press).
[35]E. Mazur, H. van Houten, and J. J. M. Beenakker, Physica A **130**, 505 (1985).
[36]P. G. van Ditzhuyzen, B. J. Thijsse, L. K. van der Meij, L. J. F. Hermans, and H. F. P. Knaap, Physica A **88**, 53 (1977).
[37]I. P. French and T. E. Arnold, Jr., J. Mol. Spectrosc. **27**, 218 (1968).
[38]B. T. Berendts and A. Dymanus, J. Chem. Phys. **48**, 1361 (1968); **49**, 2632 (1968).
[39]R. A. J. Keijser, K. D. van den Hout, M. De Groot, H. F. P. Knaap, Physica **75**, 515 (1974).
[40]R. Holmes, G. R. Jones, and R. Lawrence, J. Chem. Phys. **41**, 2955 (1964).
[41]G. J. Prangsma, A. H. Alberga, and J. J. M. Beenakker, Physica **64**, 278 (1973).